Inorg. Chem. **2007**, *46*, 2105–2114

Self-Assembly and Characterization of Cyano-Bridged Bimetallic [Ln–Fe] and [Ln–Co] Complexes (Ln = La, Pr, Nd and Sm). Nature of the Magnetic Interactions between the Ln^{3+} and Fe^{3+} Ions

Wen-Tong Chen,[†] Guo-Cong Guo,*[,†] Ming-Sheng Wang,[†] Gang Xu,[†] Li-Zhen Cai,[†] Takashiro Akitsu,[‡] Motoko Akita-Tanaka,[||] Akiyuki Matsushita,[§] and Jin-Shun Huang[†]

State Key Laboratory of Structural Chemistry, Fujian Institute of Research on the Structure of Matter, Chinese Academy of Sciences, Fuzhou, Fujian 350002, P. R. China, Department of Chemistry, Faculty of Science and Technology, Keio University, 3-14-1 Hiyoshi, Kohoku-ku, Yokohama, Kanagawa, 223-8522, Japan, Institute for Molecular Science, 38 Nishigonaka, Myodaiji, Okazaki, Aichi 444-8585, Japan, and National Institute for Materials Science, 1-2-1 Sengen, Tsukuba, Ibaraki 305-0047, Japan

Received August 25, 2006

Two structural series, including seven isomorphous heterodinuclear complexes, $[Ln(DMSO)_4(H_2O)_3(\mu\text{-}CN)M(CN)_5]\cdot H_2O$ ([La–Fe] (**1**), [Pr–Fe] (**2**), [Pr–Co] (**3**), [Nd–Fe] (**4**), [Nd–Co] (**5**), [Sm–Fe] (**6**) and [Sm–Co] (**7**)), and seven isostructural 2-D stairlike cyano-bridged bimetallic assemblies, $[Ln(DMSO)_2(H_2O)(\mu\text{-}CN)_4M(CN)_2]_n$ ($[La–Fe]_n$ (**8**), $[Pr–Fe]_n$ (**9**), $[Pr–Co]_n$ (**10**), $[Nd–Fe]_n$ (**11**), $[Nd–Co]_n$ (**12**), $[Sm–Fe]_n$ (**13**) and $[Sm–Co]_n$ (**14**)) (DMSO = dimethylsulfoxide), have been rationally prepared by a facile approach, a ball-milling method, and characterized by X-ray diffraction and magnetic measurements. The isomorphous structures, in conjunction with the diamagnetism of the Co^{3+} and La^{3+} ions, allow an approximation to the nature of coupling between the iron(III) and lanthanide(III) ions in the Ln^{3+}–Fe^{3+} complexes. The Ln^{3+}–Fe^{3+} interaction is ferromagnetic for the dinuclear [Pr–Fe] (**2**), [Nd–Fe] (**4**), and [Sm–Fe] (**6**) systems and for the 2-D $[Pr–Fe]_n$ (**9**), $[Nd–Fe]_n$ (**11**), and $[Sm–Fe]_n$ (**13**) assemblies.

Introduction

Recently, much attention has been devoted to the design and syntheses of molecule-based magnetic materials composed of cyano-bridged bimetallic assemblies because of their remarkable magnetic, magnetic-optical, and optoelectronic properties.[1] Since 1976, a series of 3-D cyano-bridged bimetallic assemblies of Prussian blue analogues, derived from the reactions of $[M(CN)_6]^{n-}$ (M = transition metal atom) and simple metal ions, have been synthesized and studied structurally and magnetically.[2] However, the difficulty in obtaining single crystals suitable for X-ray diffraction analysis impedes the investigation of the 3-D assemblies. Furthermore, the face-centered cubic structures (based on powder XRD results) of the 3-D assemblies usually result in low or no magnetic anisotropy.[2] To overcome these problems, one strategy is to incorporate organic ligands into the 3-D assemblies to increase its solubility and afford hybrid Prussian blue complexes. Now, many hybrid Prussian blue assemblies (4f−3d and 3d−3d) with low dimensionality have been obtained via the reaction of $[M(CN)_6]^{n-}$ anions with metal−organic complex cations.[3,4] Most of these assemblies are prepared by conventional solution reaction method or sovothermal approach. Notably, 4f−3d hybrid Prussian blue assemblies are relatively rare and poorly investigated,[3] in comparison with the numerous 3d−3d hybrid Prussian blue assemblies which have been well studied structurally and magnetically.[4] To our knowledge, most of the 4f−3d hybrid

* To whom correspondence should be addressed. Fax: 86 591 83714946. E-mail: gcguo@ms.fjirsm.ac.cn.
[†] State Key Laboratory of Structural Chemistry.
[‡] Keio University.
[||] Institute for Molecular Science.
[§] National Institute for Materials Science.

(1) (a) Mallah, T.; Thiébaut, S.; Verdaguer, M.; Veillet, P. *Science* **1993**, *262*, 1554. (b) Entley, W. R.; Girolami, G. S. *Science* **1995**, *268*, 397. (c) Verdaguer, M. *Science* **1996**, *272*, 698. (d) Sato, O.; Iyoda, T.; Fujishima, A.; Hashimoto, K. *Science* **1996**, *271*, 49. (e) Sato, O.; Iyoda, T.; Fujishima, A.; Hashimoto, K. *Science* **1996**, *272*, 704. (f) Holmes, S. M.; Girolami, G. S. *J. Am. Chem. Soc.* **1999**, *121*, 5593.

(2) For example, see: (a) Hulliger, F.; Landolt, M.; Vetsch, H. *J. Solid State Chem.* **1976**, *18*, 283. (b) Gadet, V.; Mallah, T.; Castro, I.; Verdaguer, M. *J. Am. Chem. Soc.* **1992**, *114*, 9213. (c) Hatlevik, Ø.; Buschmann, W. E.; Zhang, J.; Manson, J. L.; Miller, J. S. *Adv. Mater.* **1999**, *11*, 914. (d) Margadonna, S.; Prassides, K.; Fitch, A. N. *Angew. Chem., Int. Ed.* **2004**, *43*, 6316.

10.1021/ic061609p CCC: $37.00
Published on Web 02/14/2007

Prussian blue assemblies are isolated or 1-D structures, while 2-D systems[3a−3e,3i] have been rarely documented thus far.

Generally, little is known about the nature of the exchange interactions of lanthanide ions either with one another or with other magnetic groups. The ground state of the Ln^{3+} ion, with the exception of Gd^{3+}, has a first-order angular momentum, which prevents the use of a spin-only Hamiltonian for isotropic exchange and makes it difficult to study the magnetic behaviors of the 4f−3d systems. To solve this problem, Costes et al.[5] introduced a new approach that gives information on the type of exchange interaction (ferro- or antiferromagnetic) by determination of the magnetic behaviors of a corresponding complex in which the second spin carrier is substituted by a diamagnetic analogue. Thereafter, Figuerola et al.[3g] proposed a more empirical approach, which is used to obtain new insights into the nature of the Ln^{3+}−Fe^{3+} interaction by comparison of the magnetic susceptibility data of isomorphous Ln^{3+}−Fe^{3+} and Ln^{3+}−Co^{3+} complexes, together with the magnetic behaviors of the La^{3+}−Fe^{3+} complex, to take the anisotropy of the Ln^{3+} and Fe^{3+} ions into account. To date, several studies, using these approaches, on the nature of the magnetic interaction of the 4f−3d hybrid Prussian blue assemblies have been reported Most of the examples are dinuclear,[3g] trinuclear,[6] and 1-D[7] complexes, but only one 2-D example, $[Nd(bpym)(H_2O)_4Fe(CN)_6]\cdot 3H_2O$, has been documented.[3c]

We recently employed a strategy to control the structure in the solid state, which combines elements of the design, to crystal engineering and the study of magnetic behaviors. This strategy can effectively adjust the molar ratio of the reactants and solvents with ball-milling method,[3i,8] and as a result, we have successfully and easily synthesized many novel 4f−3d hybrid Prussian blue assemblies. The present work focuses on the study of the nature of the magnetic interaction of two series of 4f−3d hybrid Prussian blue assemblies, belonging to two homologous families, respectively. In this context, we report the self-assembly and characterization of seven isomorphous heterodinuclear complexes, $[Ln(DMSO)_4(H_2O)_3(\mu\text{-}CN)M(CN)_5]\cdot H_2O$ ([La−Fe] (**1**), [Pr−Fe] (**2**), [Pr−Co] (**3**), [Nd−Fe] (**4**), [Nd−Co] (**5**), [Sm−Fe] (**6**) and [Sm−Co] (**7**)), and seven isostructural 2-D cyano-bridged bimetallic 4f−3d assemblies, $[Ln(DMSO)_2(H_2O)(\mu\text{-}CN)_4M(CN)_2]_n$ ($[La-Fe]_n$ (**8**), $[Pr-Fe]_n$ (**9**), $[Pr-Co]_n$ (**10**), $[Nd-Fe]_n$ (**11**), $[Nd-Co]_n$ (**12**), $[Sm-Fe]_n$ (**13**) and $[Sm-Co]_n$ (**14**)), which were prepared by a facile ball-milling method. The isomorphous structures and the diamagnetism of the La^{3+} and Co^{3+} ions allow an approximation of the nature of the coupling between the Ln^{3+} and Fe^{3+} ions in the [Ln−Fe] complexes.

Experimental Section

Measurements. Elemental analyses of carbon, hydrogen, nitrogen, and sulfur were carried out with an Elementar Vario EL. Infrared spectra were obtained with a PE Spectrum-One FT-IR spectrometer using KBr discs. Variable-temperature magnetic susceptibility and field dependence magnetization measurements of the title complexes on polycrystalline samples were performed on an MPMS-XL and PPMS 9T Quantum Design SQUID magnetometer. All data were corrected for diamagnetism estimated from Pascal's constants.

Syntheses. All starting materials, except for $LnCl_3\cdot 6H_2O$, were commercially available and were used without further purification. $LnCl_3\cdot 6H_2O$ was prepared from the reaction of lanthanide oxide with a concentrated hydrochloric acid solution.

$[Ln(DMSO)_4(H_2O)_3(\mu\text{-}CN)Fe(CN)_5]\cdot H_2O$ (La (1), Pr (2), Nd (4), and Sm (6)). The four [Ln−Fe] complexes were prepared by grinding a mixture of $LnCl_3\cdot 6H_2O$ (1 mmol), $K_3[Fe(CN)_6]$ (1 mmol, 329 mg), and DMSO (2 mL) in a sealed agate container for 2 h with the ball-milling method. The resulting mixture was extracted

(3) For example, see: (a) Kou, H.-Z.; Gao, S.; Jin, X. L. *Inorg. Chem.* **2001**, *40*, 6295. (b) Kou, H.-Z.; Gao, S.; Sun, B.-W.; Zhang, J. *Chem. Mater.* **2001**, *13*, 1431. (c) Ma, B.-Q.; Gao, S.; Su, G.; Xu, G.-X. *Angew. Chem., Int. Ed.* **2001**, *40*, 434. (d) Yang, C.; Guo, G.-C.; Ma, H.-W.; Liu, J.-C.; Zhang, X.; Zheng, F.-K.; Lin, S.-H.; Zhou, G.-W.; Mao, J.-G.; Huang, J.-S. *Chin. J. Struct. Chem.* **2001**, *20*, 229. (e) Liang, S.-H.; Che, Y.-X.; Zheng, J.-M. *Jiegou Huaxue (Chin.) (Chin. J. Struct. Chem.)* **2005**, *24*, 7. (f) Li, J.-R.; Cai, L.-Z.; Zou, R.-Q.; Zhou, G.-W.; Guo, G.-C.; Bu, X.-H.; Huang, J.-S. *Acta Crystallogr. E* **2002**, *58*, m686. (g) Figuerola, A.; Diaz, C.; Ribas, J.; Tangoulis, V.; Granell, J.; Lloret, F.; Mahia, J.; Maestro, M. *Inorg. Chem.* **2003**, *42*, 641. (h) Li, J.-R.; Cai, L.-Z.; Guo, G.-C.; Bu, X.-H.; Huang, J.-S. *Acta Crystallogr. E* **2004**, *60*, m259. (i) Chen, W.-T.; Wang, M.-S.; Cai, L.-Z.; Xu, G.; Akitsu, T.; Akita-Tanaka, M.; Guo, G.-C.; Huang, J.-S. *Cryst. Growth Des.* **2006**, *6*, 1738. (j) Colacio, E.; Ghazi, M.; Stoeckli-Evans, H.; Lloret, F.; Moreno, J. M.; Perez, C. *Inorg. Chem.* **2001**, *40*, 4876. (k) Moore, J. G.; Lochner, E. J.; Ramsey, C.; Dalal, N. S.; Stiegman, A. E. *Angew. Chem., Int. Ed.* **2003**, *42*, 2741. (l) Tokoro, H.; Ohkoshi, S.; Matsuda, T.; Hashimoto, K. *Inorg. Chem.* **2004**, *43*, 5231. (m) Saha, M. K.; Lloret, F.; Bernal, I. *Inorg. Chem.* **2004**, *43*, 1969. (n) Berlinguette, C. P.; Dragulescu-Andrasi, A.; Sieber, A.; Galan-Mascaros, J. R.; Gudel, H.-U.; Achim, C.; Dunbar, K. R. *J. Am. Chem. Soc.* **2004**, *126*, 6222. (o) Kohler, F. H.; Lescouezec, R. *Angew. Chem., Int. Ed. Engl.* **2004**, *43*, 2571. (p) Li, G. M.; Sato, O.; Akitsu, T.; Einaga, Y. *J. Solid. State. Chem.* **2004**, *177*, 3835. (q) Hozumi, T.; Hashimoto, K.; Ohkoshi, S. *J. Am. Chem. Soc.* **2005**, *127*, 3864. (r) Ikeda, S.; Hozumi, T.; Hashimoto, K.; Ohkoshi, S. *Dalton Trans.* **2005**, 2120. (s) Saha, M. K.; Morón, M. C.; Palacio, F.; Bernal, I. *Inorg. Chem.* **2005**, *44*, 1354. (t) Bonadio, F.; Senna, M. C.; Ensling, J.; Sieber, A.; Neels, A.; Stoeckli-Evans, H.; Decurtins, S. *Inorg. Chem.* **2005**, *44*, 969. (u) Shek, I. P. Y.; Yeung, W.-F.; Lau, T.-C.; Zhang, J.; Gao, S.; Szeto, L.; Wong, W.-T. *Eur. J. Inorg. Chem.* **2005**, 364. (v) Artemkina, S. B.; Naumov, N. G.; Virovets, A. V.; Fedorov, V. E. *Eur. J. Inorg. Chem.* **2005**, 142. (w) Withers, J. R.; Ruschmann, C.; Bojang, P.; Parkin, S.; Holmes, S. M. *Inorg. Chem.* **2005**, *44*, 352.

(4) For example, see: (a) Ohba, M.; Maruono, N.; Ōawa, H.; Enoki, T.; Latour, J.-M. *J. Am. Chem. Soc.* **1994**, *116*, 11566. (b) Fu, D. G.; Chen, J.; Tan, X. S.; Jiang, L. J.; Zhang, S. W.; Zheng, P. J.; Tang, W. X. *Inorg. Chem.* **1997**, *36*, 220. (c) Van Langenberg, K.; Batten, S. R.; Berry, K. J.; Hockless, D. C. R.; Moubaraki, B.; Murray, K. S. *Inorg. Chem.* **1997**, *36*, 5006. (d) Dunbar, K. R.; Heintz, R. A. *Prog. Inorg. Chem.* **1997**, *45*, 283. (e) Colacio, E.; Domínguez-Vera, J. M.; Ghazi, M.; Kivekäs, R.; Klinga, M.; Moreno, J. M. *Chem. Commun.* **1998**, 1071. (f) Marvilliers, A.; Parsons, S.; Rivière, E.; Audière, J.-P.; Mallah, T. *Chem. Commun.* **1999**, 2217. (g) Smith, J. A.; Galán-Mascarós, J. R.; Clérac, R.; Dunbar, K. R. *Chem. Commun.* **2000**, 1077. (h) Figuerola, A.; Diaz, C.; El Fallah, M. S.; Ribas, J.; Maestro, M.; Mahía, J. *Chem. Commun.* **2001**, 1204. (i) Smith, J. A.; Galán-Mascarós, J.-R.; Clérac, R.; Sun, J.-S.; Ouyang, X.; Dunbar, K. R. *Polyhedron* **2001**, *20*, 1727.

(5) Costes, J. P.; Dahan, F.; Dupuis, A.; Laurent, J. P. *Chem.—Eur. J.* **1998**, *4*, 1616.

(6) Figuerola, A.; Ribas, J.; Llunell, M.; Casanova, D.; Maestro, M.; Alvarez, S.; Diaz, C. *Inorg. Chem.* **2005**, *44*, 6939.

(7) (a) Figuerola, A.; Diaz, C.; Ribas, J.; Tangoulis, V.; Sangregorio, C.; Gatteschi, D.; Maestro, M.; Mahía, J. *Inorg. Chem.* **2003**, *42*, 5274. (b) Figuerola, A.; Ribas, J.; Casanova, D.; Maestro, M.; Alvarez, S.; Diaz, C. *Inorg. Chem.* **2005**, *44*, 6949.

(8) To determine the effect of the ball-milling method, some control experiments have been done using both the ball-milling and conventional solution methods. The results shown that the 2-D complexes can be easily synthesized and reproduced via the ball-milling method, while they are hardly obtained via the conventional solution method.

with 10 mL of distilled water. The filtrate was left to stand at room temperature for several days, and crystals suitable for X-ray analysis were obtained from the aqueous solution. Yield: 55 (**1**), 46 (**2**), 65 (**4**), 69% (**6**). Anal. Calcd for **1**, $C_{14}H_{32}FeLaN_6O_8S_4$: C, 22.84; H, 4.35; N, 11.42; S, 17.40. Found: C, 22.26; H, 4.23; N, 11.16; S, 17.02. IR peaks (KBr, cm^{-1}): 3393 (vs), 2135 (vs), 2115 (vs), 1658 (s), 1630 (vs), 1440 (m), 1423 (m), 1320 (m), 1011 (vs), 963 (s), 670 (m), 417 (m). Anal. Calcd for **2**, $C_{14}H_{32}FeN_6O_8PrS_4$: C, 22.78; H, 4.34; N, 11.39; S, 17.36. Found: C, 22.32; H, 4.22; N, 11.15; S, 17.01. IR peaks (KBr, cm^{-1}): 3392 (vs), 2124 (s), 2115 (vs), 1660 (s), 1630 (vs), 1423 (m), 1323 (m), 1000 (vs), 964 (s), 671 (s), 417(w). Anal. Calcd for **4**, $C_{14}H_{32}FeN_6NdO_8S_4$: C, 22.68; H, 4.32; N, 11.34; S, 17.28. Found: C, 22.12; H, 4.20; N, 11.09; S, 16.90. IR peaks (KBr, cm^{-1}): 3434 (vs), 2133 (s), 2120 (vs), 1661 (s), 1625 (vs), 1424 (m), 1319 (m), 1005 (vs), 963 (s), 675 (s), 419 (w). Anal. Calcd for **6**, $C_{14}H_{32}FeN_6O_8S_4Sm$: C, 22.49; H, 4.28; N, 11.25; S, 17.14. Found: C, 22.03; H, 4.37; N, 11.49; S, 17.51. IR peaks (KBr, cm^{-1}): 3382 (vs), 2161 (s), 2130 (vs), 1662 (s), 1640 (vs), 1493 (m), 1432 (m), 1377 (s), 1243 (m), 1115 (m), 1056 (w), 679 (s), 430 (s).

$[Ln(DMSO)_4(H_2O)_3(\mu\text{-}CN)Co(CN)_5]\cdot H_2O$ (Pr (3), Nd (5), and Sm (7)). The three [Ln−Co] complexes were obtained by the same procedure that was used for **1** with $K_3[Co(CN)_6]$ instead of $K_3[Fe(CN)_6]$. Yield: 75 (**3**), 78 (**5**), 64% (**7**). Anal. Calcd for **3**, $C_{14}H_{32}CoN_6O_8PrS_4$: C, 22.69; H, 4.32; N, 11.34; S, 17.28. Found: C, 22.25; H, 4.18; N, 11.11; S, 17.62. IR peaks (KBr, cm^{-1}): 3400 (vs), 2159 (s), 2130 (vs), 1649 (s), 1415 (s), 1318 (m), 1006 (vs), 958 (s), 716 (m), 411 (w). Anal. Calcd for **5**, $C_{14}H_{32}CoN_6NdO_8S_4$: C, 22.58; H, 4.30; N, 11.29; S, 17.21. Found: C, 22.05; H, 4.17; N, 11.02; S, 17.56. IR peaks (KBr, cm^{-1}): 3532 (vs), 3368 (vs), 2141 (vs), 2129 (s), 1651 (s), 1624 (s), 1417 (m), 1320 (m), 1009 (vs), 965 (s), 615 (m), 434 (s). Anal. Calcd for **7**, $C_{14}H_{32}CoN_6O_8S_4Sm$: C, 22.40; H, 4.27; N, 11.20; S, 17.07. Found: C, 21.95; H, 4.10; N, 11.73; S, 17.52. IR peaks (KBr, cm^{-1}): 3434 (vs), 2142 (vs), 1682 (s), 1629 (s), 1416 (m), 1321 (m), 1015 (vs), 987 (s), 943 (s), 718 (m), 423(s).

$[Ln(DMSO)_2(H_2O)(\mu\text{-}CN)_4Fe(CN)_2]_n$ (La (8), Pr (9), Nd (11), and Sm (13)). These $[Ln-Fe]_n$ complexes were synthesized by the same procedure that was used for **1** with 0.50 mL of DMSO instead of 2 mL. Yield: 52 (**8**), 56 (**9**), 63 (**11**), 79% (**13**). Anal. Calcd for **8**, $C_{10}H_{14}FeLaN_6O_3S_2$: C, 22.85; H, 2.67; N, 15.99; S, 12.19. Found: C, 22.35; H, 2.58; N, 15.42; S, 12.64. IR peaks (KBr, cm^{-1}): 3366 (vs), 2133 (vs), 2115 (vs), 1658 (s), 1631 (s), 1418 (s), 1401 (s), 1322 (m), 1011 (vs), 962 (vs), 670 (s), 403 (s). Anal. Calcd for **9**, $C_{10}H_{14}FeN_6O_3PrS_2$: C, 22.76; H, 2.66; N, 15.93; S, 12.14. Found: C, 22.25; H, 2.58; N, 15.37; S, 12.46. IR peaks (KBr, cm^{-1}): 3431 (vs), 2137 (vs), 2129 (vs), 2066 (m), 1631 (s), 1401 (m), 1320 (m), 1003 (vs), 960 (s), 600 (w), 423(m). Anal. Calcd for **11**, $C_{10}H_{14}FeN_6NdO_3S_2$: C, 22.64; H, 2.64; N, 15.84; S, 12.07. Found: C, 22.17; H, 2.53; N, 15.30; S, 11.81. IR peaks (KBr, cm^{-1}): 3391 (vs), 2127 (vs), 2115 (vs), 1661 (s), 1423 (m), 1322 (m), 1001 (vs), 962 (s), 670 (w), 426 (m). Anal. Calcd for **13**, $C_{10}H_{14}FeN_6O_3S_2Sm$: C, 22.38; H, 2.61; N, 15.66; S, 11.93. Found: C, 22.93; H, 2.50; N, 15.22; S, 11.50. IR peaks (KBr, cm^{-1}): 3379 (vs), 2138 (vs), 2129 (vs), 1627 (s), 1401 (m), 1319 (m), 1004 (vs), 962 (s), 601 (w), 422 (m).

$[Ln(DMSO)_2(H_2O)(\mu\text{-}CN)_4Co(CN)_2]_n$ (Pr (10), Nd (12), and Sm (14)). These $[Ln-Co]_n$ complexes were synthesized by the same procedure that was used for the $[Ln-Fe]_n$ complexes with $K_3[Co(CN)_6]$ instead of $K_3[Fe(CN)_6]$. Yield: 71 (**10**), 68 (**12**), 63% (**14**). Anal. Calcd for **10**, $C_{10}H_{14}CoN_6O_3PrS_2$: C, 22.63; H, 2.64; N, 15.84; S, 12.07. Found: C, 22.01; H, 2.55; N, 15.35; S, 12.43. IR peaks (KBr, cm^{-1}): 3450 (vs), 2144 (vs), 2122 (vs), 1635 (m), 1400 (w), 1003 (s), 961 (s), 602 (w), 435(s). Anal. Calcd for **12**, $C_{10}H_{14}CoN_6NdO_3S_2$: C, 22.49; H, 2.62; N, 15.74; S, 11.99. Found: C, 21.93; H, 2.53; N, 15.37; S, 12.51. IR peaks (KBr, cm^{-1}): 3368 (vs), 2141 (vs), 2129 (vs), 1651 (s), 1417 (m), 1320 (m), 1009 (vs), 965 (vs), 615 (w), 434 (m). Anal. Calcd for **14**, $C_{10}H_{14}CoN_6O_3S_2Sm$: C, 22.22; H, 2.59; N, 15.56; S, 11.85. Found: C, 22.70; H, 2.69; N, 15.11; S, 11.43. IR peaks (KBr, cm^{-1}): 3436 (vs), 2146 (vs), 2132 (vs), 1631 (s), 1417 (m), 1318 (m), 1003 (vs), 962 (s), 800 (m), 436 (s).

Crystallographic Studies. The intensity data sets were collected on Rigaku Mercury CCD (**1**−**8**, **10**, and **12**−**14**) and Siemens SMART CCD (**9** and **11**) X-ray diffractometers with graphite-monochromated Mo Kα radiation ($\lambda = 0.71073$ Å) using an ω scan technique. CrystalClear (**1**−**8**, **10**, and **12**−**14**) and Siemens SAINT (**9** and **11**) softwares were used for data reduction and empirical absorption corrections.[9] The structures were solved by direct methods using the Siemens SHELXTL, version 5, package of crystallographic software.[10] The difference Fourier maps based on these atomic positions yield the other non-hydrogen atoms. The hydrogen atoms, except for those on the lattice water molecules in which one of the two H atoms for each water molecule was generated from the difference Fourier maps, were generated theoretically, allowed to ride on their respective parent atoms, and included in the structure factor calculations with assigned isotropic thermal parameters, but they were not refined. Additionally, the hydrogen atoms on the disordered DMSO ligands were not generated because of the disorder of the sulfur atoms. The structures were refined using a full-matrix least-squares refinement on F^2. All atoms, except for the hydrogen atoms, were refined anisotropically.

Results and Discussion

Generally, increasing the dimensionality of a structure may enhance and improve bulk magnetic properties.[3c,11] Hence, the syntheses of higher-dimensional 4f−3d hybrid Prussian blue complexes have attracted great attention. Hybrid Prussian blue complexes are often synthesized via a solution reaction method, mostly yielding discrete 4f−3d complexes with the coordination environment of the Ln^{3+} ions being easily saturated by solvent ligands,[3g,12,15c] which prevents more CN^- groups from the $[M(CN)_6]^{n-}$ block from bridging the Ln^{3+} ions to form 1-, 2-, or 3-D structures. To obtain higher-dimensional 4f−3d hybrid Prussian blue complexes, the amount of solvent used in the reactive system should be reduced as much as possible. Our strategy is to employ the ball-milling reaction method to effectively control the molar ratio of reactants, organic ligands, and solvents. As a result, we successfully synthesized a series of 2-D cyano-bridged 4f−3d hexacyanometallates.[3i]

The IR spectra of **1**−**14** show sharp bands in the range of 2100−2200 cm^{-1} that are attributed to the C≡N stretching modes. The splitting of $\nu_{C\equiv N}$ suggests the presence of both

(9) (a) *CrystalClear*, version 1.35; Rigaku Corporation: The Woodlands, TX, 2002. (b) *SAINT Software Reference Manual*; Siemens Energy & Automation Inc.: Madison, WI, 1994.
(10) *SHELXTL*, version 5; Siemens Energy & Automation Inc.: Madison, WI, 1994.
(11) (a) Kou, H.-Z.; Gao, S.; Ma, B.-Q.; Liao, D.-Z. *Chem. Commun.* **2000**, 1309. (b) Inoue, K.; Kikuchi, K.; Ohba, M.; Kawa, H. *Angew. Chem., Int. Ed.* **2003**, *42*, 4810.
(12) Li, J.-R.; Cai, L.-Z.; Zheng, Y.; Guo, G.-C.; Bu, X.-H.; Huang, J.-S. *Chin. J. Inorg. Chem.* **2003**, *19*, 91.

Table 1. Crystal Parameters for **1**−**14**

	1	**2**	**3**
formula	$C_{14}H_{32}FeLaN_6O_8S_4$	$C_{14}H_{32}FeN_6O_8PrS_4$	$C_{14}H_{32}CoN_6O_8PrS_4$
fw	735.46	737.46	740.54
color	greenish−yellow	green	green
cryst size (mm^3)	0.40 × 0.30 × 0.20	0.45 × 0.30 × 0.10	0.16 × 0.14 × 0.05
cryst syst	monoclinic	monoclinic	monoclinic
space group	$P2_1/n$	$P2_1/n$	$P2_1/n$
a (Å)	14.985(1)	14.917(3)	14.882(5)
b (Å)	13.751(1)	13.701(3)	13.661(4)
c (Å)	15.384(2)	15.386(3)	15.292(5)
β (deg)	108.075(4)	108.384(4)	108.049(3)
V ($Å^3$)	3013.5(5)	2984(1)	2956(2)
Z	4	4	4
$2\theta_{max}$ (deg)	50	50	50
reflns collected	19 124	18 250	19 092
independent, observed reflns (R_{int})	5185, 3410 (0.0512)	5244, 4818 0.0300)	5191, 4169 (0.0433)
d_{calcd} (g/cm^3)	1.621	1.641	1.664
μ (mm^{-1})	2.200	2.423	2.517
T (K)	293(2)	293(2)	293(2)
F(000)	1476	1484	1488
R1, wR2	0.0471, 0.1053	0.0445, 0.1245	0.0619, 0.1889
S	1.004	1.008	1.006
largest and mean Δ/σ	0.003, 0	0.002, 0	0.002, 0
$\Delta\rho$(max/min) ($e/Å^3$)	0.543/−1.097	0.838/−0.772	0.758/−0.645

	4	**5**	**6**	**7**
formula	$C_{14}H_{32}FeN_6NdO_8S_4$	$C_{14}H_{32}CoN_6NdO_8S_4$	$C_{14}H_{32}FeN_6O_8S_4Sm$	$C_{14}H_{32}CoN_6O_8S_4Sm$
fw	735.46	743.87	746.90	749.98
color	yellow	colorless	green	colorless
cryst size (mm^3)	0.48 × 0.45 × 0.35	0.45 × 0.30 × 0.10	0.40 × 0.40 × 0.05	0.42 × 0.40 × 0.20
cryst syst	monoclinic	monoclinic	monoclinic	monoclinic
space group	$P2_1/n$	$P2_1/n$	$P2_1/n$	$P2_1/n$
a (Å)	14.899(5)	14.740(3)	14.870(8)	14.819(3)
b (Å)	13.693(5)	13.574(3)	13.644(7)	13.617(3)
c (Å)	15.399(5)	15.123(3)	15.369(8)	15.296(3)
β (deg)	108.498(4)	107.633(4)	108.648(8)	108.338(2)
V ($Å^3$)	2979(2)	2884(1)	2955(3)	2930(1)
Z	4	4	4	4
$2\theta_{max}$ (deg)	50	50	50	50
refls collected	18 443	18 306	18 093	17 754
independent, observed reflns (R_{int})	5244, 3171 (0.0685)	5031, 4052 (0.0404)	5193, 2693 (0.1000)	5096, 3575 (0.0315)
d_{calcd} (g/cm^3)	1.652	1.713	1.679	1.700
μ (mm^{-1})	2.534	2.691	2.786	2.880
T (K)	293(2)	293(2)	293(2)	293(2)
F(000)	1488	1492	1496	1500
R1, wR2	0.0433, 0.0904	0.0310, 0.0747	0.0640, 0.1111	0.0298, 0.0577
S	1.007	0.998	0.995	0.992
largest and mean Δ/σ	0.002, 0	0.003, 0	0.002, 0	0.003, 0
$\Delta\rho$(max/min) ($e/Å^3$)	1.111/−0.498	1.003/−0.751	1.129/−0.996	0.487/−0.490

bridged and terminal C≡N$^-$ ligands. The strong bands at 900−1100 cm^{-1} are assigned to the S═O (DMSO) stretching vibrations.

Crystal Structures. A summary of the crystallographic data and structure analyses for **1**−**14** is presented in Table 1, and selected bond lengths and bond angles are given in Table 2.

[Ln(DMSO)$_4$(H$_2$O)$_3$(μ-CN)M(CN)$_5$]·H$_2$O (1−7). The X-ray diffraction analysis reveals that complexes **1**−**7** are isomorphous, and only complex **7** is discussed in detail.

An ORTEP drawing of **7** is shown in Figure 1. The structure of **7** consists of neutral [Sm(DMSO)$_4$(H$_2$O)$_3$(μ-CN)-Co(CN)$_5$] species and lattice water molecules. The Sm^{3+} ion is eight coordinate being bound by four O atoms from four DMSO molecules (av Sm−O$_{DMSO}$ = 2.372(2) Å), three O atoms from three water molecules (av Sm−O$_{H2O}$ = 2.463-(2) Å), and one N atom from one bridging CN$^-$ group (Sm−N = 2.577(2) Å), yielding a distorted square anti-prism with the top and bottom planes defined by N6, O21, O41, O31 and O1W, O11, O3W, O2W atoms, respectively. The Co^{3+} ion is coordinated by six cyanide groups to form an approximately regular octahedron with the Co−C and C≡N bond distances in the ranges of 1.880(2)−1.906(2) and 1.138(3)−1.158(3) Å, respectively, which are in good agreement with those reported in ref 13. The cyano-bridged Sm···Co distance is 5.598(1) Å, comparable with that found in an analog, [Sm(DMF)$_4$(H$_2$O)$_3$(μ-CN)Co(CN)$_5$]·H$_2$O.[3g] As shown in Figure S1 i the Supporting Information, the [Sm-(DMSO)$_4$(H$_2$O)$_3$(μ-CN)Co(CN)$_5$] species are linked to each other via hydrogen bonds between the terminal cyanide

(13) For example, see: (a) Marvaud, V.; Decroix, C.; Scuiller, A.; Guyard-Duhayon, C.; Vaissermann, J.; Gonnet, F.; Verdaguer, M. *Chem.*−*Eur. J.* **2003**, *9*, 1677. (b) Marvaud, V.; Decroix, C.; Scuiller, A.; Tuyeras, F.; Guyard-Duhayon, C.; Vaissermann, J.; Marrot, M.; Gonnet, F.; Verdaguer, M. *Chem.*−*Eur. J.* **2003**, *9*, 1692. (c) Eckhardt, R.; Hanika-Heidl, H.; Fischer, R. D. *Chem.*−*Eur. J.* **2003**, *9*, 1795.

Table 1. Continued

	8	**9**	**10**
formula	$C_{10}H_{14}FeLaN_6O_3S_2$	$C_{10}H_{14}FeN_6O_3PrS_2$	$C_{10}H_{14}CoN_6O_3PrS_2$
fw	525.15	527.15	530.23
color	yellow	brown	light green
cryst size (mm^3)	0.30 × 0.30 × 0.20	0.26 × 0.24 × 0.04	0.25 × 0.23 × 0.15
cryst system	monoclinic	monoclinic	monoclinic
space group	*P*2/*n*	*P*2/*n*	*P*2/*n*
a (Å)	7.921(1)	7.8106(3)	7.786(1)
b (Å)	10.752(1)	10.6967(4)	10.629(1)
c (Å)	11.250(2)	11.1162(1)	11.078(1)
β (deg)	97.007(3)	97.035(2)	96.692(6)
V ($Å^3$)	950.9(2)	921.74(5)	910.5(2)
Z	2	2	2
$2\theta_{max}$ (deg)	50	50	50
reflns collected	6069	2946	5617
independent, observed reflns (R_{int})	1674, 1397 (0.0502)	1626, 1384 (0.0488)	1573, 1507 (0.0304)
d_{calcd} (g/cm^3)	1.834	1.899	1.934
μ (mm^{-1})	3.217	3.644	3.803
T (K)	293(2)	293(2)	293(2)
F(000)	510	514	516
R1, wR2	0.0423, 0.1088	0.0568, 0.1338	0.0309, 0.0760
S	1.016	1.007	0.993
largest and mean Δ/σ	0, 0	0.001, 0	0.003, 0
$\Delta\rho$(max/min) ($e/Å^3$)	1.569/−1.221	1.229/−1.196	1.290/−0.633

	11	**12**	**13**	**14**
formula	$C_{10}H_{14}FeN_6NdO_3S_2$	$C_{10}H_{14}CoN_6NdO_3S_2$	$C_{10}H_{14}FeN_6O_3S_2Sm$	$C_{10}H_{14}CoN_6O_3S_2Sm$
fw	530.48	533.56	536.59	539.67
color	brown	green	brown	colorless
cryst size (mm^3)	0.44 × 0.28 × 0.14	0.15 × 0.15 × 0.10	0.28 × 0.06 × 0.05	0.13 × 0.07× 0.05
cryst syst	monoclinic	monoclinic	monoclinic	monoclinic
space group	*P*2/*n*	*P*2/*n*	*P*2/*n*	*P*2/*n*
a (Å)	7.822(1)	7.772(4)	7.764(1)	7.7719(6)
b (Å)	10.707(1)	10.614(6)	10.687(1)	10.6882(9)
c (Å)	11.098(1)	11.043(8)	11.049(1)	11.0306(9)
β (deg)	96.905(1)	96.592(2)	97.084(9)	97.033(3)
V ($Å^3$)	922.7(2)	904.9(9)	909.8(2)	909.39(13)
Z	2	2	2	2
$2\theta_{max}$ (deg)	50	50	50	50
reflns collected	2586	5332	5868	5735
independent, observed reflns (R_{int})	1613, 1286 (0.0382)	1570, 1513 (0.0308)	1609, 1489 (0.0474)	1592, 1488 (0.0623)
d_{calcd} (g/cm^3)	1.909	1.958	1.959	1.971
μ (mm^{-1})	3.813	4.003	4.241	4.357
T (K)	293(2)	293(2)	293(2)	293(2)
F(000)	516	518	520	522
R1, wR2	0.0591, 0.1402	0.0332, 0.0819	0.0375, 0.0870	0.0532, 0.1198
S	0.994	1.018	1.007	1.003
largest and mean Δ/σ	0.001, 0	0.001, 0	0, 0	0.001, 0
$\Delta\rho$(max/min) ($e/Å^3$)	1.866/−2.048	1.260/−1.200	0.923/−0.926	1.083/−0.906

groups and coordinated and lattice water molecules to form a 3-D supramolecular hydrogen-bonding network.

It is noteworthy that the bridging bond angle of Fe−C−N in **4** is 175.0(2)°, which is similar to that in the DMF-containing analog (176.89[14a] and 179.40°[14b]). However, the bridging bond angle of Nd−N−C in **4** is 170.3(2)°, which is obviously larger than that in the DMF-containing analog (164.88[14a] and 162.37°[14b]).

$[Ln(DMSO)_2(H_2O)(\mu\text{-}CN)_4M(CN)_2]_n$ (8−14). Complexes **8**−**14** are isostructural, and complex **11** is presented as an example here.

An ORTEP drawing of **11** is shown in Figure 2. The structure of **11** consists of neutral stairlike layers. The Nd^{3+} ion is seven coordinate being bound by two O atoms from two DMSO molecules (av Nd−O_{DMSO} = 2.355(3) Å), one O atom from one water molecule (Nd−O_{H2O} = 2.364(4) Å), and four N atoms from four bridging CN^- groups (av Nd−N = 2.550(4) Å), yielding a distorted pentagonal bipyramid with a pentagon defined by O11, N2A (1 − *x*, 2 − *y*, 1 − *z*), N4B (2 − *x*, 2 − *y*, 1 − *z*), O21 and O1W atoms, and two apical atoms N6 and N5C (*x*, *y*, 1 + *z*). The Fe^{3+} ion is coordinated by six cyanide groups to form an approximately regular octahedron with the Fe−C and C≡N bond distances in the normal ranges of 1.930(4)−1.938(3) and 1.115(5)−1.152(5) Å, respectively. The cyano-bridged Nd···Fe distances are in the range of 5.5568(7)−5.6349(7) Å and are comparable to those found in the literature.[14] The $[Fe(CN)_6]^{3-}$ unit connects to three $[Nd(DMSO)_2(H_2O)]^{3+}$ units through three equatorial CN^- groups, and vice versa, forming an approximately rectangular "grid" of Nd_2Fe_2 with four edges in the range of 5.5568(7)−5.6349(7) Å, which interlink along the *c* direction to form a "step". The steps connect to each

(14) (a) Li, J.-R.; Guo, G.-C.; Wang, M.-S.; Zhou, G.-W.; Bu, X.-H.; Huang, J.-S. *Chin. J. Struct. Chem.* **2003**, *22*, 182. (b) Li, G. M.; Akitsu, T.; Sato, O.; Einaga, Y. *J. Am. Chem. Soc.* **2003**, *125*, 12396. (c) Chen, W.-T.; Cai, L.-Z.; Wu, A.-Q.; Guo, G.-C.; Huang, J.-S. *Chin. J. Struct. Chem.* **2004**, *23*, 1282.

Table 2. Selected Bond Lengths (Å) and Angles (deg)[a]

	[La−Fe] **1**	[Pr−Fe] **2**	[Pr−Co] **3**	[Nd−Fe] **4**	[Nd−Co] **5**	[Sm−Fe] **6**	[Sm−Co] **7**
Ln(1)−O(11)	2.460(2)	2.421(2)	2.413(2)	2.401(2)	2.406(1)	2.375(2)	2.388(2)
Ln(1)−O(21)	2.443(2)	2.407(2)	2.415(2)	2.408(2)	2.401(2)	2.359(2)	2.378(2)
Ln(1)−O(31)	2.444(2)	2.399(2)	2.392(2)	2.351(2)	2.401(1)	2.372(2)	2.362(2)
Ln(1)−O(41)	2.439(3)	2.398(3)	2.401(4)	2.385(2)	2.386(2)	2.358(2)	2.361(2)
Ln(1)−O(1W)	2.549(2)	2.494(2)	2.498(2)	2.483(2)	2.478(1)	2.454(2)	2.458(2)
Ln(1)−O(2W)	2.589(2)	2.535(2)	2.549(2)	2.534(2)	2.533(1)	2.499(2)	2.498(1)
Ln(1)−O(3W)	2.521(2)	2.462(2)	2.471(2)	2.459(2)	2.470(1)	2.436(2)	2.432(2)
Ln(1)−N(6)	2.667(3)	2.621(3)	2.621(3)	2.605(2)	2.611(2)	2.562(2)	2.577(2)
M(1)−C(1)	1.938(3)	1.943(2)	1.896(3)	1.944(3)	1.900(2)	1.938(2)	1.899(2)
M(1)−C(2)	1.921(3)	1.930(2)	1.898(3)	1.914(3)	1.882(2)	1.926(3)	1.880(2)
M(1)−C(3)	1.942(3)	1.946(3)	1.898(3)	1.940(3)	1.905(2)	1.939(3)	1.898(2)
M(1)−C(4)	1.937(3)	1.936(3)	1.892(4)	1.926(3)	1.890(2)	1.928(3)	1.891(2)
M(1)−C(5)	1.930(3)	1.928(3)	1.897(4)	1.911(3)	1.892(2)	1.928(3)	1.899(2)
M(1)−C(6)	1.949(3)	1.954(3)	1.899(4)	1.956(3)	1.913(2)	1.956(3)	1.906(2)
M(1)−C(6)−N(6)	175.1(2)	175.0(2)	173.9(3)	175.0(2)	174.9(2)	175.3(2)	175.0(2)
Ln(1)−N(6)−C(6)	169.8(2)	169.9(2)	170.0(3)	170.3(2)	170.1(2)	170.6(2)	169.7(2)

	[La−Fe]$_n$ **8**	[Pr−Fe]$_n$ **9**	[Pr−Co]$_n$ **10**	[Nd−Fe]$_n$ **11**	[Nd−Co]$_n$ **12**	[Sm−Fe]$_n$ **13**	[Sm−Co]$_n$ **14**
Ln(1)−O(11) (×2)	2.407(3)	2.363(3)	2.365(2)	2.355(3)	2.363(1)	2.333(3)	2.348(2)
Ln(1)−O(1W)	2.409(6)	2.373(5)	2.361(3)	2.364(4)	2.395(2)	2.327(5)	2.359(4)
Ln(1)−N(1)#1 (×2)	2.583(4)	2.523(4)	2.533(2)	2.540(4)	2.511(2)	2.478(4)	2.471(4)
Ln(1)−N(3) (×2)	2.630(4)	2.573(4)	2.563(2)	2.560(3)	2.544(1)	2.521(4)	2.525(3)
M(1)−C(1) (×2)	1.945(4)	1.917(4)	1.885(2)	1.930(4)	1.891(2)	1.943(4)	1.897(3)
M(1)−C(2) (×2)	1.930(4)	1.924(4)	1.888(2)	1.936(4)	1.900(1)	1.931(4)	1.908(3)
M(1)−C(3) (×2)	1.942(4)	1.947(4)	1.898(2)	1.938(3)	1.902(1)	1.950(4)	1.926(3)
M(1)−C(1)−N(1)	178.6(4)	177.9(4)	178.9(2)	178.4(3)	179.8(1)	177.4(4)	179.2(3)
M(1)−C(2)−N(2)	177.7(4)	177.4(4)	176.3(2)	176.6(3)	176.8(1)	176.0(4)	176.9(3)
M(1)−C(3)−N(3)	177.5(4)	177.8(4)	177.5(2)	177.8(3)	176.4(1)	178.0(4)	177.9(3)
Ln(1)−N(1)−C(1)#2	169.3(4)	168.9(4)	169.5(2)	169.2(3)	169.1(1)	170.2(4)	169.0(3)
Ln(1)−N(3)−C(3)	170.7(3)	169.7(3)	170.8(2)	170.8(3)	170.1(1)	170.3(4)	170.9(3)

[a] Symmetry codes: #1 $x - 1/2, -y + 1, z - 1/2$; #2 $-x + 1, -y + 1, -z + 1$.

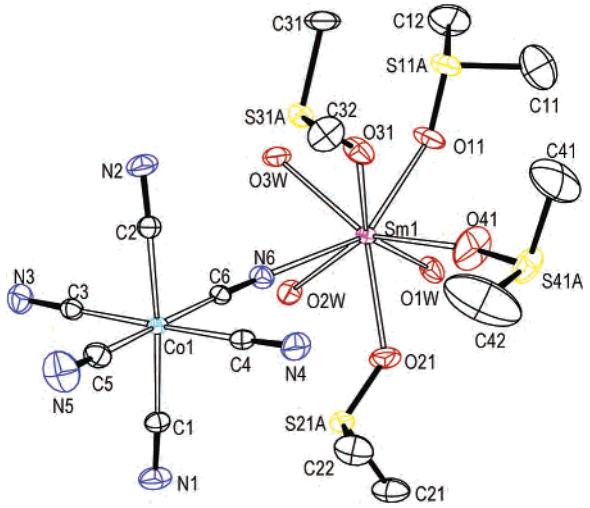

Figure 1. ORTEP drawing of **7** with 30% thermal ellipsoids. The lattice water molecules and disordered S11B, S21B, S31B, and S41B atoms are omitted for clarity.

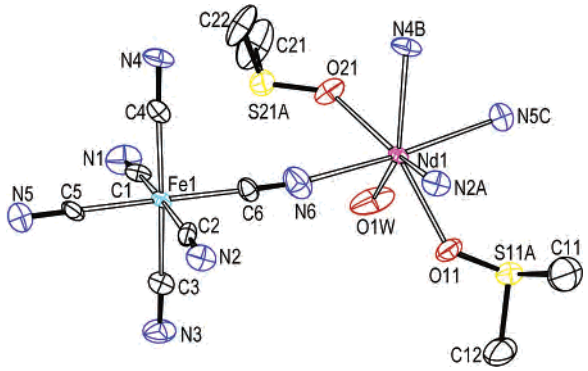

Figure 2. ORTEP drawing of **11** with 40% thermal ellipsoids. The disordered S11B and S21B atoms are omitted for clarity. Symmetry codes: (A) $1 - x, 2 - y, 1 - z$; (B) $2 - x, 2 - y, 1 - z$; (C) $x, y, 1 + z$.

other through the axial CN^- groups of $[Fe(CN)_6]^{3-}$ units to form a "stair" running along the *a* direction (Figure 3). The stairlike topologies in **8**−**14** are the second examples in hexacyanometallates.[3d] The shortest interlayer Nd···Fe distance is 7.7151(9) Å, obviously longer than those of the intralayer. Between the adjacent layers, the terminal cyanide groups interact with the coordinating O1W water molecules through O−H···N hydrogen bonds to form a 3-D supramolecular hydrogen-bonding network (Figure S2).

The cyano-bridged lanthanide hexacyanometallates generally have a formula of $Ln(L)_x(H_2O)_yM(CN)_6$ (L = assistant ligands or terms as the third ligands, $x = 1-5$, $y = 1-5$), of which several examples with DMSO as the assistant ligand have been reported.[3d,3e,14c,15] Noteworthily, by means of exploiting the ball-milling method to effectively control the molar ratio of reactants and solvents, we have easily prepared a series of cyano-bridged lanthanide hexacyanometallates

(15) (a) Liang, S.-H.; Che, Y.-X.; Zheng, J.-M. *Jiegou Huaxue (Chin.) (Chin. J. Struct. Chem.)* **2004**, *23*, 1226. (b) Zhou, B.-C.; Kou, H.-Z.; He, Y.; Wang, R.-J.; Li, Y.-D.; Wang, H.-G. *Chin. J. Chem.* **2003**, *21*, 352. (c) Chen, W.-T.; Cai, L.-Z.; Wu, A.-Q.; Guo, G.-C.; Huang, J.-S.; Dong, Z.-C.; Matsushita, A. *Chin. J. Inorg. Chem.* **2004**, *20*, 693.

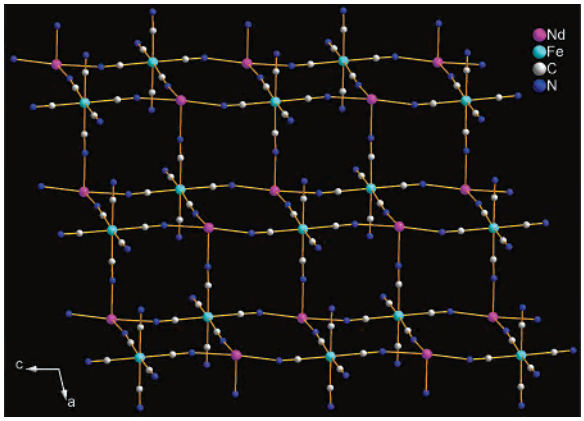

Figure 3. Stairlike 2-D layer of **11** with the DMSO and water molecules omitted for clarity.

with a formula of $Ln(DMSO)_x(H_2O)_yM(CN)_6 \cdot nH_2O$ ($x = 1-5$), that is, $\{[Gd(DMSO)(DMF)_3(H_2O)_3](\mu\text{-}CN)[Fe(CN)_5]\} \cdot 2H_2O$[15c] ($x = 1$), $[Ln(DMSO)_2(H_2O)(\mu\text{-}CN)_4M(CN)_2]_n$ (**8**−**14**) ($x = 2$), $[Gd(DMSO)_3(H_2O)_4(\mu\text{-}CN)Co(CN)_5] \cdot H_2O$, $[Pr(DMSO)_3(H_2O)_3(\mu\text{-}CN)_2Fe(CN)_4]_n \cdot nH_2O$[16] ($x = 3$), $[Ln(DMSO)_4(H_2O)_3(\mu\text{-}CN)M(CN)_5] \cdot H_2O$ (**1**−**7**) ($x = 4$), and $[Nd(DMSO)_5(H_2O)_2](\mu\text{-}CN)[Fe(CN)_5]$[14c] ($x = 5$).

Magnetic Studies. Magnetic measurements were performed for the present complexes. The Ln^{3+} (with the exception of the La^{3+}) and Fe^{3+} ions have a first-order angular momentum, which prevents the use of a spin-only Hamiltonian for isotropic exchange. Therefore, for a [Ln−Fe] system, the deviation of the magnetic susceptibility with respect to the Curie law is entirely caused by the thermal population of the Ln^{3+} Stark components and the anisotropy of Fe^{3+} ion, respectively. Generally, the magnetic property of a [Ln−Fe] complex is reflected by three factors, a possible $Ln^{3+}-Fe^{3+}$ magnetic coupling ($\Delta\chi_M T$) and the contributions of the Ln^{3+} ($\chi_M T^{[Ln]}$) and Fe^{3+} ($\chi_M T^{[Fe]}$) ions, which can be denoted as $\chi_M T^{[Ln-Fe]} = \Delta\chi_M T + \chi_M T^{[Ln]} + \chi_M T^{[Fe]}$. In this equation, the contributions of $\chi_M T^{[Ln]}$ and $\chi_M T^{[Fe]}$ in the [Ln−Fe] complex can be approximately replaced by the $\chi_M T^{[Ln-Co]}$ from the isomorphous [Ln−Co] complex and the $\chi_M T^{[La-Fe]}$ from the isomorphous [La−Fe] complex, respectively, because of the diamagnetic nature of the Co^{3+} and La^{3+} ions. To gain the insight into the nature of the $Ln^{3+}-Fe^{3+}$ magnetic interaction, three isomorphous complexes ([Ln−Fe], [Ln−Co], and [La−Fe]) and their magnetic data are necessary. Similar to the approach proposed by Figuerola et al.,[3g,6,7b] an increase of the $\Delta\chi_M T$ with the lowered temperature suggests that the $Ln^{3+}-Fe^{3+}$ magnetic coupling in the [Ln−Fe] complex is ferromagnetic, while a decrease indicates it is antiferromagnetic. The comparison of the magnetization of the coupled system with that of the corresponding uncorrelated spin systems at low temperature affords another way to distinguish the sign of the coupling for 4f−3d complexes. More explicitly, if the *M* versus *H* curve of the coupled system is running above the curve of the noncorrelated system, that is, the sum of the [Ln−Co] and [La−Fe] magnetization curves, a ferromagnetic interaction within the molecular spin system is revealed, whereas the reverse would be an antiferromagnetic interaction.[17]

Dinuclear Complexes $[Pr(DMSO)_4(H_2O)_3(\mu\text{-}CN)Fe(CN)_5] \cdot H_2O$ (2) and $[Pr(DMSO)_4(H_2O)_3(\mu\text{-}CN)Co(CN)_5] \cdot H_2O$ (3). The temperature dependence of $\chi_M T$ for the [Pr−Co] complex is shown at the left of Figure 4. At 300 K, the $\chi_M T^{[Pr-Co]}$ value is 1.36 emu mol^{-1} K, slightly smaller than the expected value in the free-ion approximation for one isolated Pr^{3+} ion (1.60 emu mol^{-1} K) and decreases with temperature to 0.09 emu mol^{-1} K at 2 K. The temperature dependence of $\chi_M T$ for the [Pr−Fe] complex is also shown at the left of Figure 4. The $\chi_M T^{[Pr-Fe]}$ value is 1.83 emu mol^{-1} K at 300 K, while it decreases with temperature to 0.45 emu mol^{-1} K at 2 K. From 300 to 4 K, the $\Delta\chi_M T$ versus *T* curve is a horizontal line, indicating that no exchange interaction is active down to this temperature. Below 4 K, $\Delta\chi_M T$ slightly increases with the lowered temperature, indicative of a weak ferromagnetic interaction between the Pr^{3+} and Fe^{3+} ions in **2**. The experimental magnetization of the [Pr−Fe] complex at 2 K (Figure 4 right) shows that the deviation at high fields is higher than that of the uncorrelated spin system, corroborating a ferromagnetic coupling.

Dinuclear Complexes $[Nd(DMSO)_4(H_2O)_3(\mu\text{-}CN)Fe(CN)_5] \cdot H_2O$ (4) and $[Nd(DMSO)_4(H_2O)_3(\mu\text{-}CN)Co(CN)_5] \cdot H_2O$ (5). A plot of the $\chi_M T$ values of the [Nd−Fe] (**4**) and [Nd−Co] (**5**) complexes is shown at the left of Figure 5, together with the $\chi_M T$ of [La−Fe] and $\Delta\chi_M T$. At 300 K, the $\chi_M T$ of [Nd−Co] is about 1.41 emu mol^{-1} K, close to the expected value for one isolated Nd^{3+} ion (1.63 emu mol^{-1} K), and decreases with temperature to 0.47 emu mol^{-1} K at 2 K. The $\chi_M T$ of [Nd−Fe] is 1.96 emu mol^{-1} K at 300 K and decreases with the temperature to 0.84 emu mol^{-1} K at 12 K followed by a slight increase to 0.95 emu mol^{-1} K at 2 K. In the temperature span of 300−15 K, $\Delta\chi_M T$ decreases with temperature, indicating an antiferromagnetic exchange interaction down to 15 K. From 15 to 2 K, $\Delta\chi_M T$ increases with decreasing temperature, suggesting a ferromagnetic interaction at the low temperature. Furthermore, the magnetization of [Nd−Fe] at 2 K (Figure 5 right) is obviously higher than that of the uncorrelated spin system, also in accordance with the ferromagnetic coupling.

Dinuclear Complexes $[Sm(DMSO)_4(H_2O)_3(\mu\text{-}CN)Fe(CN)_5] \cdot H_2O$ (6) and $[Sm(DMSO)_4(H_2O)_3(\mu\text{-}CN)Co(CN)_5] \cdot H_2O$ (7). A plot of the $\chi_M T$ values of the [Sm−Fe] (**6**) and [Sm−Co] (**7**) complexes is shown at the left of Figure 6. The $\chi_M T$ value of [Sm−Co] is 0.27 emu mol^{-1} K at 300 K, and it decreases with temperature to 0.04 emu mol^{-1} K at 2 K. For the [Sm−Fe] complex, the $\chi_M T$ at 300 K is 0.69 emu mol^{-1} K, and it decreases with the temperature to 0.19 emu mol^{-1} K at 7 K and then increases abruptly to 0.27 emu mol^{-1} K at 2 K. From 300 to 7 K, $\Delta\chi_M T$ decreases with decreasing temperature, which indicates that a weak antiferromagnetic interaction occurs between the Sm^{3+} and Fe^{3+} ions in **6**. From 7 to 2 K, $\Delta\chi_M T$ increases with the temperature, suggesting a ferromagnetic interaction at low temperature. The experimental magnetization of [Sm−Fe]

(16) Cambridge Crystallographic Data Centre, CCDC 286206 and 286207, http://www.ccdc.cam.ac.uk.

(17) Sutter, J. P.; Khan, M. L.; Khan, O. *Adv. Mater.* **1999**, *11*, 863.

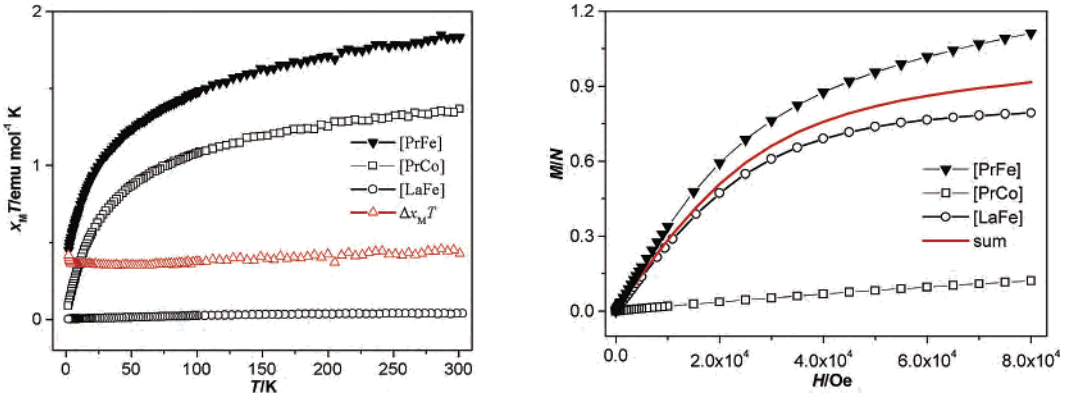

Figure 4. (left) Thermal dependence of $\chi_M T^{[Pr-Fe]}$ (**2**), $\chi_M T^{[Pr-Co]}$ (**3**), $\chi_M T^{[La-Fe]}$ (**1**) at 0.5 T, and $\Delta\chi_M T = \chi_M T^{[Pr-Fe]} - \chi_M T^{[Pr-Co]} - \chi_M T^{[La-Fe]}$. (right) Magnetization vs H (2 K) of $M^{[Pr-Fe]}$, $M^{[Pr-Co]}$, $M^{[La-Fe]}$, and sum $= M^{[Pr-Co]} + M^{[La-Fe]}$.

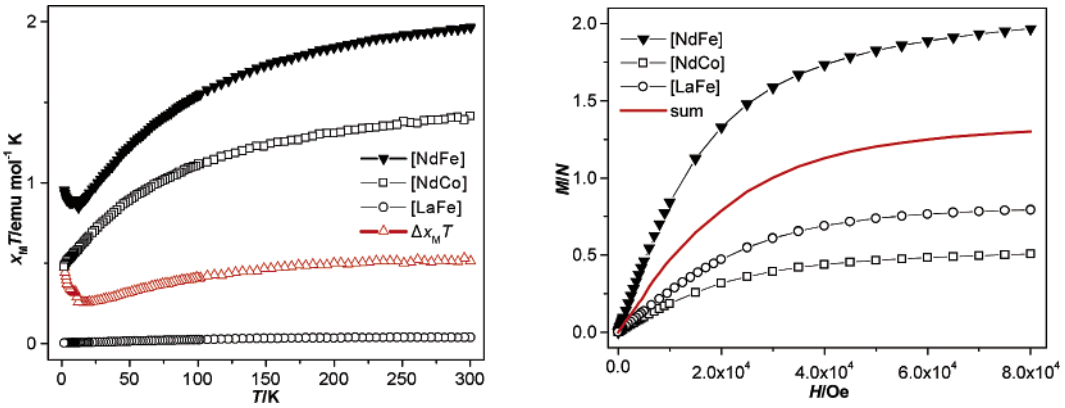

Figure 5. (left) Thermal dependence of $\chi_M T^{[Nd-Fe]}$ (**4**), $\chi_M T^{[Nd-Co]}$ (**5**), $\chi_M T^{[La-Fe]}$ (**1**) at 0.5 T, and $\Delta\chi_M T = \chi_M T^{[Nd-Fe]} - \chi_M T^{[Nd-Co]} - \chi_M T^{[La-Fe]}$. (right) Magnetization vs H (2 K) of $M^{[Nd-Fe]}$, $M^{[Nd-Co]}$, $M^{[La-Fe]}$, and sum $= M^{[Nd-Co]} + M^{[La-Fe]}$.

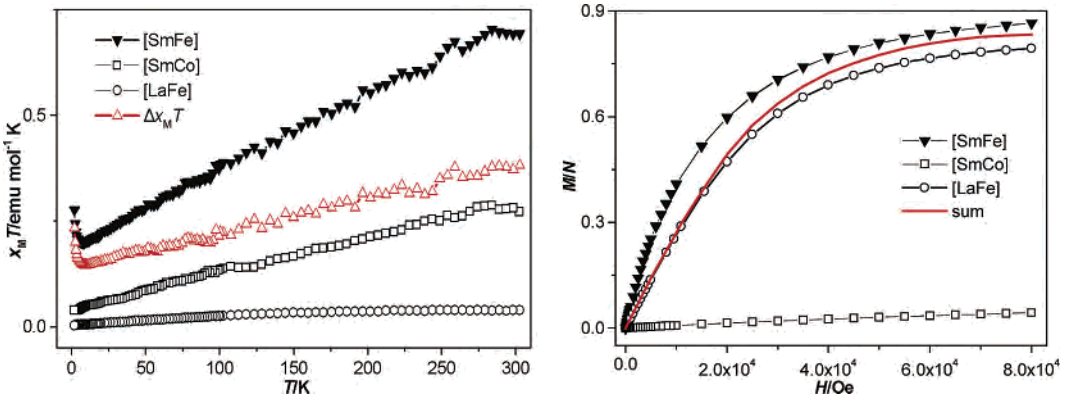

Figure 6. (left) Thermal dependence of $\chi_M T^{[Sm-Fe]}$ (**6**), $\chi_M T^{[Sm-Co]}$ (**7**), $\chi_M T^{[La-Fe]}$ (**1**) at 0.5 T, and $\Delta\chi_M T = \chi_M T^{[Sm-Fe]} - \chi_M T^{[Sm-Co]} - \chi_M T^{[La-Fe]}$. (right) Magnetization vs H (2 K) of $M^{[Sm-Fe]}$, $M^{[Sm-Co]}$, $M^{[La-Fe]}$, and sum $= M^{[Sm-Co]} + M^{[La-Fe]}$.

at 2 K (Figure 6 right) is slightly higher than that of the uncorrelated spin system, suggesting a weak ferromagnetic interaction.

2-D Complexes $[Pr(DMSO)_2(H_2O)(\mu\text{-}CN)_4Fe(CN)_2]_n$ (9) and $[Pr(DMSO)_2(H_2O)(\mu\text{-}CN)_4Co(CN)_2]_n$ (10). A plot of the $\chi_M T$ values of the $[Pr-Fe]_n$ (**9**), $[Pr-Co]_n$ (**10**), and $[La-Fe]_n$ (**8**) complexes is shown at the left of Figure 7, in combination with $\Delta\chi_M T$. When the temperature is lowered to about 6 K, the $\Delta\chi_M T$ decreases with temperature (Figure 7 left), indicating a weak antiferromagnetic interaction. The $\Delta\chi_M T$ slowly increases below that temperature, implying a weak ferromagnetic interaction between the Pr^{3+} and Fe^{3+} ions in **9** below 6 K. Magnetization measurements (Figure 7 right) also prove the above argument because the experimental magnetization of $[Pr-Fe]_n$ is higher than that of the uncorrelated spin system.

2-D Complexes $[Nd(DMSO)_2(H_2O)(\mu\text{-}CN)_4Fe(CN)_2]_n$ (11) and $[Nd(DMSO)_2(H_2O)(\mu\text{-}CN)_4Co(CN)_2]_n$ (12). The case of $[Nd-Fe]_n$ is investigated in Figure 8. At 300 K, the $\chi_M T$ value of $[Nd-Fe]_n$ is 1.88 emu mol^{-1} K; it slowly decreases to 1.26 emu mol^{-1} K at 5 K (Figure 8 left). The $\chi_M T$ value of $[Nd-Co]_n$ is 1.51 emu mol^{-1} K at 300 K, close to the expected value for one isolated Nd^{3+} ion (1.63 emu mol^{-1} K), and it smoothly decreases to 0.43 emu mol^{-1} K at 5 K. From 300 to 5 K, $\Delta\chi_M T$ increases with temperature, reflecting a possible ferromagnetic character of the $Nd^{3+}-$

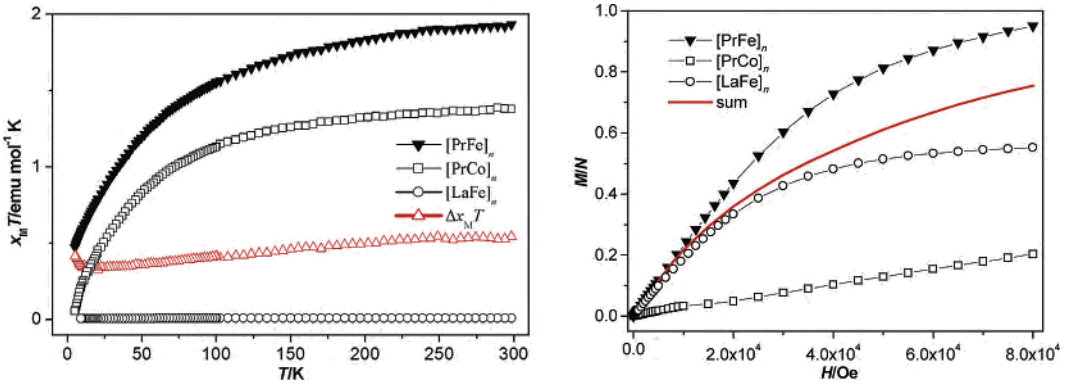

Figure 7. (left) Thermal dependence of $\chi_M T^{[Pr-Fe]_n}$ (**9**), $\chi_M T^{[Pr-Co]_n}$ (**10**), $\chi_M T^{[La-Fe]_n}$ (**8**) at 0.5 T, and $\Delta\chi_M T = \chi_M T^{[Pr-Fe]_n} - \chi_M T^{[Pr-Co]_n} - \chi_M T^{[La-Fe]_n}$. (right) Magnetization vs H (2 K) of $M^{[Pr-Fe]_n}$, $M^{[Pr-Co]_n}$, $M^{[La-Fe]_n}$, and sum $= M^{[Pr-Co]_n} + M^{[La-Fe]_n}$.

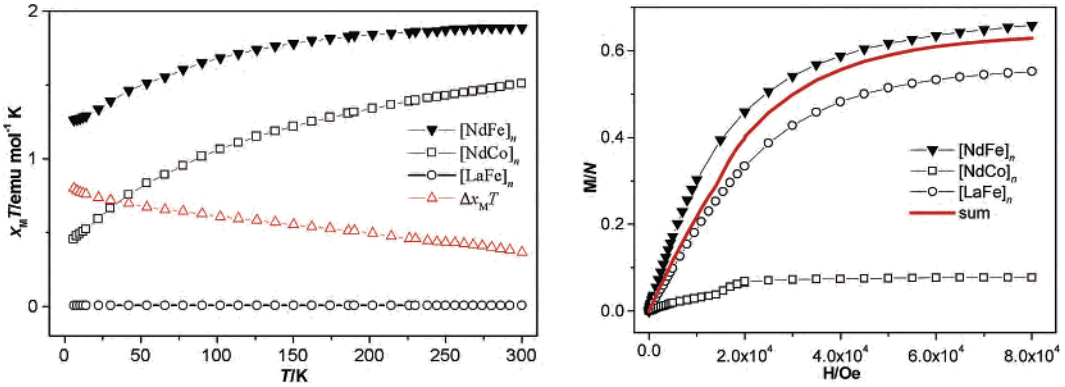

Figure 8. (left) Thermal dependence of $\chi_M T^{[Nd-Fe]_n}$ (**11**), $\chi_M T^{[Nd-Co]_n}$ (**12**), $\chi_M T^{[La-Fe]_n}$ (**8**) at 0.5 T, and $\Delta\chi_M T = \chi_M T^{[Nd-Fe]_n} - \chi_M T^{[Nd-Co]_n} - \chi_M T^{[La-Fe]_n}$. (right) Magnetization vs H (2 K) of $M^{[Nd-Fe]_n}$, $M^{[Nd-Co]_n}$, $M^{[La-Fe]_n}$, and sum $= M^{[Nd-Co]_n} + M^{[La-Fe]_n}$.

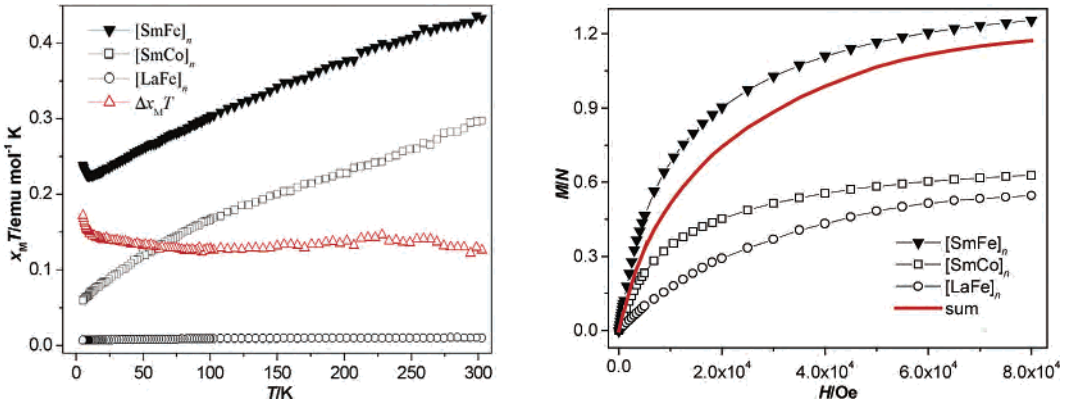

Figure 9. (left) Thermal dependence at 0.5 T of $\chi_M T^{[Sm-Fe]_n}$ (**13**), $\chi_M T^{[Sm-Co]_n}$ (**14**), $\chi_M T^{[La-Fe]_n}$ (**8**), and $\Delta\chi_M T = \chi_M T^{[Sm-Fe]_n} - \chi_M T^{[Sm-Co]_n} - \chi_M T^{[La-Fe]_n}$. (right) Magnetization vs H (2 K) of $M^{[Sm-Fe]_n}$, $M^{[Sm-Co]_n}$, $M^{[La-Fe]_n}$, and sum $= M^{[Sm-Co]_n} + M^{[La-Fe]_n}$.

Fe^{3+} interaction. The weak ferromagnetic interaction is reflected in the magnetization data (Figure 8 right), where at 2 K, the experimental $[Nd-Fe]_n$ curve is slightly higher than that of the uncorrelated spin system.

2-D Complexes $[Sm(DMSO)_2(H_2O)(\mu\text{-}CN)_4Fe(CN)_2]_n$ (13) and $[Sm(DMSO)_2(H_2O)(\mu\text{-}CN)_4Co(CN)_2]_n$ (14). For the case of $[Sm-Fe]_n$, the temperature dependence of $\chi_M T^{[Sm-Fe]_n}$ (**13**), $\chi_M T^{[Sm-Co]_n}$ (**14**), and $\chi_M T^{[La-Fe]_n}$ (**8**) is shown in the left of Figure 9, jointly with $\Delta\chi_M T$. Between 300 and 100 K, $\Delta\chi_M T$ is almost a horizontal line, suggesting no obvious interaction between the spin carriers in this temperature range. From approximately 100 to 5 K, the $\Delta\chi_M T$ value increases with decreasing temperature, clearly indicative of a ferromagnetic $Sm^{3+}-Fe^{3+}$ interaction in **13**. Furthermore, the experimental magnetization of $[Sm-Fe]_n$ at 2 K (Figure 9 right) is higher than that of the uncorrelated spin system, in agreement with the ferromagnetic coupling.

Table 3 summarizes the nature of the magnetic interaction between Ln^{3+} and the d-metal ions of the 4f−3d complexes,[3c,3g,5,6,7,18] and includes our findings concerning the dinuclear [Ln−Fe] and 2-D $[Ln-Fe]_n$ complexes. The significant differences between the previous results and the present work are the cases of Pr^{3+} and Sm^{3+} which show ferromagnetic interactions, in contrast to the previous complexes. For the case of Nd^{3+}, the interaction between the Nd^{3+} and Fe^{3+} ions is

(18) (a) Kahn, M. L.; Lecante, P.; Verelst, M.; Mathonière, C.; Kahn, O. *Chem. Mater.* **2000**, *12*, 3073. (b) Kahn, M. L.; Mathonière, C.; Kahn, O. *Inorg. Chem.* **1999**, *38*, 3692.

Table 3. Nature of the Magnetic Interaction between Ln^{3+} and Fe^{3+} or Other d-Metal Ions[a]

Ln−M	Ce	Pr	Nd	Sm	Eu	Gd	Tb	Dy	Ho	Er	Tm	Yb
Ln_2Ni_3[b]	PAF	PAF	PAF	PAF	PAF	F	F	F	F			
Ln_2Cu_3[c]	PAF	PAF	PAF	PAF	PAF	F	F	F			F	
LnCu[d]	AF	NI	AF	AF	NI	F	F	F	F	F	AF	AF
LnFe[e]	AF	NI	AF	NI	NI	AF	F	AF	F	NI	F	NI
Ln_2Fe[f]	WAF	NI	NI									
$_\infty^1$[LnFe][g]					NI		AF	AF	NI	NI	NI	
$_\infty^1$[LnFe][h]						WAF						
$_\infty^2$[LnFe][i]			F									
LnFe[j]		F	F	WF								
$_\infty^2$[LnFe][j]		F	WF	F								

[a] PAF = proposed antiferromagnetic interaction; *F* = ferromagnetic interaction; AF = antiferromagnetic interaction; WAF = weakly antiferromagnetic interaction; NI = negligible interaction; WF = weakly ferromagnetic interaction. [a] −h: [b]Ref 16a. [c] Ref 16b, [d] Ref 5. [e] Ref 3g. [f] Ref 6. [g] Ref 7b. [h] Ref 7a. [i] Ref 3c. [j] This work.

ferromagnetic in **4** and **11**, consistent with one case found in the literature[3c] but different from the other cases.[3g,5,6,18]

Conclusion

In summary, we employ a facile approach, a ball-milling reaction method, to design and control the syntheses of 14 dinuclear and 2-D cyano-bridged 4f−3d hexacyanometallates, which we have structurally and magnetically characterized. Noteworthily, the ball-milling reaction method can be extended to $LnCr(CN)_6$ systems that are not as complicated as the $LnFe(CN)_6$ analogs. Our investigations provide a new avenue for the syntheses of 2-D cyano-bridged bimetallic systems. This research on the nature of the magnetic interactions for **8**−**14** is the second example of 2-D 4f−3d hybrid Prussian blue assemblies. To gain new insights into the nature of themagnetic interactions of paramagnetic centers in 2-D f−d systems, we modified the approach that was proposed by Figuerola et al. By using this improved approach, we found that the Ln^{3+}−Fe^{3+} interaction is ferromagnetic for Ln^{3+} = Pr^{3+}, Nd^{3+}m and Sm^{3+}, but for the other lanthanide ions, further studies are necessary to synthesize and characterize new isolated dinuclear and 2-D complexes.

Acknowledgment. We gratefully acknowledge the financial support of the NSF of China (20571075, 20521101), the NSF for Distinguished Young Scientist of China (20425104), and the NSF of Fujian Province (E0510028).

Supporting Information Available: X-ray crystallographic files in CIF format for **1**−**14** and packing diagrams for **7** and **11**. This material is available free of charge via the Internet at http://pubs.acs.org.

IC061609P